






# Hyperbolic Meteoroids Impacting the Moon

J. R. Szalay<sup>1</sup> , P. Pokorný<sup>2,3</sup> , and M. Horányi<sup>4,5,6</sup> <sup>1</sup> Department of Astrophysical Sciences, Princeton University, 4 Ivy Ln., Princeton, NJ 08540, USA; [jszalay@princeton.edu](mailto:jszalay@princeton.edu)<sup>2</sup> Astrophysics Science Division, NASA Goddard Spaceflight Center, Greenbelt, MD 20771, USA<sup>3</sup> Department of Physics, The Catholic University of America, Washington, DC 20064, USA<sup>4</sup> Department of Physics, University of Colorado Boulder, 392 UCB, Boulder, CO 80309, USA<sup>5</sup> Laboratory for Atmospheric and Space Physics, 1234 Innovation Dr., Boulder, CO 80303, USA<sup>6</sup> Institute for Modeling Plasma, Atmospheres, and Cosmic Dust, 3400 Marine St., Boulder, CO 80303, USA

Received 2019 December 31; revised 2020 January 23; accepted 2020 January 29; published 2020 February 12

## Abstract

Since the discovery of the Moon’s asymmetric ejecta cloud, the origin of its sunward-canted density enhancement has not been well understood. We propose impact ejecta from meteoroids on hyperbolic trajectories ( $\beta$ -meteoroids) that hit the Moon’s sunward side could explain this unresolved asymmetry.  $\beta$ -meteoroids are submicron in size, comparable to or smaller than the regolith particles they hit, and can impact the Moon at very high speeds  $\sim 100$  km s<sup>-1</sup>. Therefore, their impact regime may differ from the significantly larger and slower sporadic meteoroids responsible for generating the bulk of the lunar impact ejecta cloud. We compare lunar impact ejecta production to  $\beta$ -meteoroid fluxes observed by multiple spacecraft. If  $\beta$ -meteoroids are able to liberate similar sized submicron particles, orbital dust detector measurements from the Lunar Dust Experiment on board the Lunar Atmosphere and Dust Environment Explorer spacecraft only need to detect one ejecta grain out of every  $10^6$   $\beta$ -meteoroid impacts to the lunar surface to explain the sunward asymmetry with this additional population. This finding suggests  $\beta$ -meteoroids may also contribute to the evolution of other airless surfaces in the inner solar system, and by extension, at exozodiacal systems.

*Unified Astronomy Thesaurus concepts:* [Circumstellar dust \(236\)](#); [Interplanetary dust \(821\)](#); [Meteoroid dust clouds \(1039\)](#); [Zodiacal cloud \(1845\)](#); [Lunar impacts \(958\)](#); [Impact phenomena \(779\)](#); [Ejecta \(453\)](#)

## 1. Introduction

The Moon is continually bombarded by meteoroids, sustaining a permanently present impact ejecta cloud (Horányi et al. 2015). The Lunar Dust Experiment (LDEX), an impact ionization dust detector (Horányi et al. 2014) on board the *Lunar Atmosphere and Dust Environment Explorer (LADEE)* mission (Elphic et al. 2014), measured the lunar ejecta cloud in a near-equatorial orbit from 2013 October to 2014 April. These measurements revealed a dynamic and structured ejecta cloud that was responsive to changes in the meteoroid flux during known meteoroid showers (Szalay & Horányi 2016a; Szalay et al. 2018). The ejecta cloud is asymmetric due to the majority of sporadic impactors hitting the Moon on its apex hemisphere (Szalay & Horányi 2015a) and its density peak is canted sunward at 6–8 local time (LT) as shown in the mission averaged ejecta cloud in Figure 1. Specifically, the apex meteoroid source (AP) is the dominant ejecta producer, which while low in flux it impacts the Moon with large speeds  $\sim 60$  km s<sup>-1</sup> centered around 6 LT. The helion (HE) and antihelion (AH) meteoroid sources impact the Moon with average speeds  $\sim 10$  km s<sup>-1</sup> around 10.3 LT and 1.7 LT, respectively, and serve to further enhance impact ejecta production on the apex hemisphere (Szalay & Horányi 2015a). A small contribution from the anti-apex source (Janches et al. 2000) was also found to potentially contribute to the dusk-side ejecta density (Szalay & Horányi 2016b). Figure 1 shows the arrival directions of these various sources, where length and width of each arrow qualitatively correspond to the characteristic speed and flux, respectively.

The HE and AH sources are a manifestation of the same population of grains on prograde orbits about the Sun with

different orbital elements than the Moon. Grains on the outbound (moving antisunward) portion of their orbits that impact the Moon form the HE source, while grains on the inbound portion form the AH source. As grains in these populations come from a large number of comets and underwent thousands of years of dynamical evolution, we can expect a random/uniform distribution of their orbital elements: arguments of pericenter, longitudes of ascending node, and mean/true anomalies. This results in an approximately equal impactor flux from the HE and AH sources (Nesvorný et al. 2011). In contrast to the large apex/anti-apex asymmetry in the ejecta cloud, the sunward enhancement of the ejecta cloud has not been well understood. The first analysis that determined the cloud structure was consistent with the HE, AH, AP sources suggested this asymmetry could be due to an annual variability of HE/AH fluxes (Szalay & Horányi 2015b). A subsequent study suggested instead an unidentified instrumental artifact or surface phenomena may be the culprit of this asymmetry (Janches et al. 2018). The “excess” impact rate was found to generally increase from 6 to 11 LT, and with the inclusion of this additional empirical source, the structure of the ejecta cloud was found to be consistent with the expectation based on a dynamic impactor flux model (Pokorný et al. 2019).

However, models of the zodiacal dust distribution do not indicate any significant asymmetry in impactor fluxes between the HE and AH sources. Additionally, there is currently no instrumental effect or surface phenomena identified that would produce such a sunward-canted asymmetry. Here, we propose an alternate hypothesis for the sunward cant of the ejecta cloud: bombardment by grains on hyperbolic trajectories escaping the solar system known as  $\beta$ -meteoroids (Zook & Berg 1975). The proposed hypothesis rests on the fact that  $\beta$ -meteoroids are one of the few truly asymmetric meteoroid sources in the solar

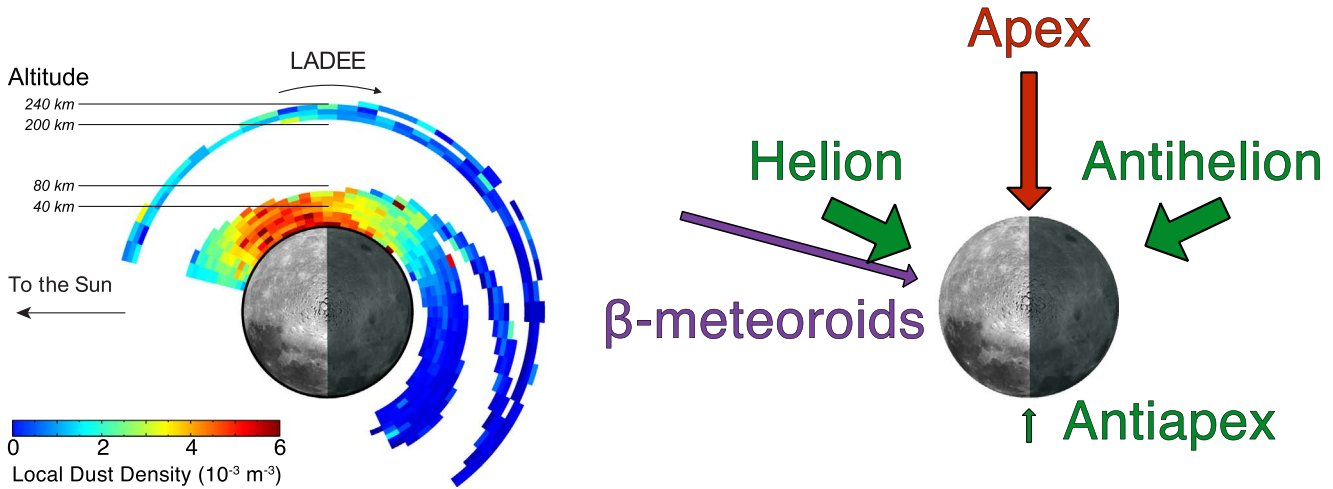


**Figure 1.** (Left) Lunar ejecta cloud observed by LDEX over the entire *LADEE* mission. (Right) Impactors in the Moon’s equatorial plane. Helion, antihelion, and anti-apex impactors are all due to impacts from meteoroids on prograde orbits. Apex impactors are from meteoroids on retrograde orbits.  $\beta$ -meteoroids impact the Moon near 11 LT as determined from analytic estimates. The length and width of each arrow qualitatively correspond to the characteristic speed and flux, respectively.

system, as unbound grains always travel away from the Sun and lack a symmetric inbound counterpart. In Section 2 we review the origins and dynamics of  $\beta$ -meteoroids. We show in Section 3 how this source could explain the observed asymmetry in the lunar ejecta cloud by comparing model predictions to the LDEX data. The implications of these results are discussed in Section 4, and we highlight our conclusions in Section 5.

## 2. $\beta$ -meteoroid Fluxes to the Moon

Dust grains shed from asteroids or comets in our zodiacal cloud have orbits that circularize and spiral in toward the Sun over long timescales due to angular momentum loss from Poynting–Robertson and solar wind drag (e.g., Burns et al. 1979). The zodiacal dust density increases as these grains get closer to the Sun (e.g., Leinert et al. 1981; Pokorný & Kuchner 2019) until they are collisionally fragmented and/or lose mass via sublimation, generating smaller grains (e.g., Mann et al. 2004). Grains in the submicron size become susceptible to radiation pressure, which opposes solar gravity with the same  $r^{-2}$  radial dependence and their orbital characteristics are set by the ratio of solar radiation pressure over gravity,  $\beta = F_R/F_G$  (Burns et al. 1979). This ratio  $\beta$  is dependent on both particle size and composition. Grains with  $\beta > 0.5$  released from circular orbits have positive orbital energy and follow hyperbolic trajectories, escaping the heliosphere in 1–10 yr. These  $\beta$ -meteoroids (Zook & Berg 1975) can attain speeds  $\sim 100 \text{ km s}^{-1}$  by the time they reach 1 au.

$\beta$ -meteoroids have been detected by multiple spacecraft: *Pioneers* 8 and 9 (Berg & Grün 1973), *Helios* (Grün et al. 1980), *Ulysses* (Wehry & Mann 1999; Wehry et al. 2004), *STEREO* (Zaslavsky et al. 2012), and *Parker Solar Probe* (*PSP*; Szalay et al. 2020; Page et al. 2020). Flux estimates (propagated to 1 au assuming an  $r^{-2}$  dependence) vary by approximately an order of magnitude, with values from *Pioneer* 8 and 9 of  $600 \text{ km}^{-2} \text{ s}^{-1}$  (Berg & Grün 1973; Grün et al. 1985), *Ulysses* of  $200 \text{ km}^{-2} \text{ s}^{-1}$  (Wehry & Mann 1999),  $10\text{--}60 \text{ km}^{-2} \text{ s}^{-1}$  (Zaslavsky et al. 2012), and *PSP* of  $30\text{--}70 \text{ km}^{-2} \text{ s}^{-1}$  (Szalay et al. 2020). The most recent measurements by *STEREO* and *PSP* were not made with a dedicated dust detector, but inferred from potential spikes

detected by electric field antenna booms. However, due to the large effective area of each spacecraft’s cross-sectional area, they are able to detect orders of magnitude more  $\beta$ -meteoroid impacts than previous observations. For *PSP*, both the impact rate profile (Szalay et al. 2020) and inferred directionality (Page et al. 2020) from impacts to the spacecraft were consistent with a dominantly  $\beta$ -meteoroid impactor population. Across the various spacecraft measurements, the total flux of  $\beta$ -meteoroids at 1 au is estimated to be  $\mathcal{F}_\beta \approx 10\text{--}600 \text{ km}^{-2} \text{ s}^{-1}$  (Berg & Grün 1973; Wehry & Mann 1999; Zaslavsky et al. 2012; Szalay et al. 2020).

To model  $\beta$ -meteoroid production, we assume they are generated at a heliocentric distance  $r_0$  and originate with the energy and angular momentum a grain in a circular orbit would have at that location (Zook & Berg 1975). Based on the conservation of their initial angular momentum and altered orbital energy to account for the reduced effective solar gravity, their speed and direction can be directly estimated as a function of distance from the Sun. For a range of  $\beta = 0.6\text{--}1.2$  and  $r_0 = 5\text{--}30$  solar radii ( $R_S$ ), we calculate  $\beta$ -meteoroid impact speed  $v_{\text{imp}}$  and location in LT to the lunar surface as a function of  $\beta$  (Figure 2).

The top panel of Figure 2 shows the  $\beta$ -meteoroid impact speed to the Moon. Grains generated closer to the Sun undergo antisunward acceleration for a longer distance due to radiation pressure on their journey to 1 au, and even though they start deeper in the gravitational well of the Sun, they attain larger impact speeds. The larger the value of  $\beta$  the more dominant radiation pressure’s repulsive force is compared to gravity’s attractive force and grains with larger  $\beta$  reach higher speeds. The bottom panel of Figure 2 shows the LT where  $\beta$ -meteoroids impact the lunar surface, accounting for the orbital motion of the Moon. Most of the  $\beta$ -meteoroid impactors are moving almost entirely in the radial direction at 1 au, hence the larger the speed the closer to the subsolar direction (12 LT)  $\beta$ -meteoroids impact the lunar surface. Their impact location is also represented with the purple  $\beta$ -meteoroid arrow in Figure 1.

## 3. Model–Data Comparison

Here, we incorporate a  $\beta$ -meteoroid impactor source into a previous model for lunar impact ejecta generated by sporadic

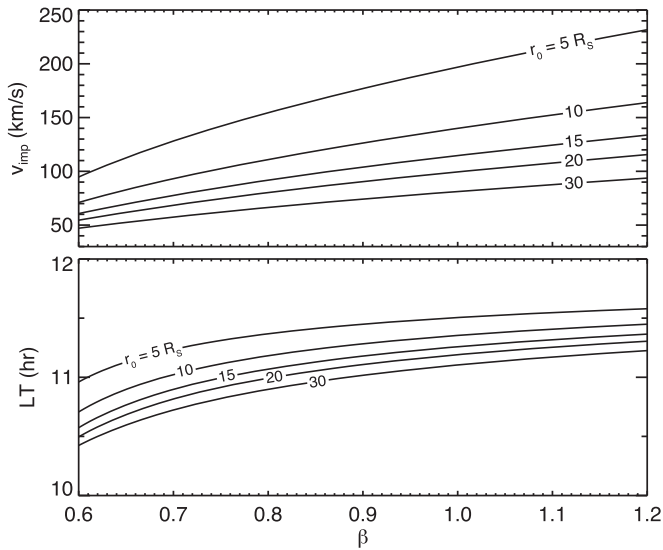


**Figure 2.** Impact speed  $v_{\text{imp}}$  (top) and location (bottom) of  $\beta$ -meteoroids reaching the lunar surface as functions of  $\beta$ . The various lines are for different semimajor axes  $r_0$  of the initial circular orbit of the parent body.

meteoroids on bound orbits (Pokorný et al. 2019). The existing dynamical model follows the individual trajectories of sporadic meteoroids released from a variety of cometary and asteroidal bodies throughout their lifetime in the solar system. Ejecta production from this dynamical model was found to be reasonably consistent with *LADEE*/*LDEX* ejecta observations, particularly on the antisunward (night) side of the Moon. We use the outputs from this model (Figure 1 in Pokorný et al. 2019) and incorporate  $\beta$ -meteoroid impactors as a collimated beam incident at 11 LT. The dynamical model accounts for the relative motion of both the Moon with respect to the Earth and the Earth with respect to the Sun, as each produces small temporal variations in impact ejecta production. For the additional  $\beta$ -meteoroid source, we do not account for these small velocity modulations as they are negligible compared to the impact speeds on the order of  $\sim 100 \text{ km s}^{-1}$  for these impactors. We assume the angular response for ejecta production is  $\cos^3(\varphi - \varphi_\beta)$  (Gault et al. 1974) as used in previous analysis for *LDEX* (e.g., Szalay & Horányi 2015a; Janches et al. 2018; Pokorný et al. 2019), where  $\varphi$  is the local time expressed in degrees and  $\varphi_\beta$  corresponds to 11 LT. The validity of this relationship is stretched even further than before, as the impactor speeds  $\sim 100 \text{ km s}^{-1}$  are much higher than both the lab experiments this relationship was determined for and the lunar ejecta data it has been applied to previously. However, without an updated relation, we utilize this result.

Figures 3 and 4 show a comparison of ejecta production, separately for the  $\beta$ -meteoroid and sporadic sources, their combined ejecta production, and the *LDEX* data for each of the 6 months *LDEX* gathered ejecta data. Both the colors and lengths of the radial color strips in Figure 3 and vertical axes in Figure 4 indicate the ejecta density at the surface,  $n_0$ . Instead of performing a more complex month-to-month fit for how much  $\beta$ -meteoroid impactor flux we would expect, for a proof of concept we use a simple constant value of  $n_{0\beta} = 1.3 \times 10^{-3} \text{ m}^{-3}$  across all months, a value that reasonably reproduces the “excess” dayside ejecta production observed by *LDEX* (Pokorný et al. 2019). While the month-to-month variation in *LDEX* data leaves different portions of each month matching or departing from the updated model, the addition of a  $\beta$ -

meteoroid source at 11 LT serves both to broaden and shift the peak density sunward, more consistent with the *LDEX* observations than the dynamical sporadic model alone. We note that this represents one iteration of the dynamical model and  $\beta$ -meteoroid model. A more comprehensive model could perform a fit by including  $\beta$ -meteoroids into the dynamical model. Additionally, *Ulysses* measurements indicate the flux of  $\beta$ -meteoroids could be variable (Wehry et al. 2004) and accounting for such a variability of the  $\beta$ -meteoroid source magnitude could also improve the fidelity of the fit. Yet, even with the simple addition of a constant  $\beta$ -meteoroid source, the sunward-canted ejecta cloud is reasonably well reproduced.

## 4. Discussion

We have shown that the addition of an impact ejecta source near 11 LT is sufficient to produce the sunward cant observed in the lunar ejecta cloud.  $\beta$ -meteoroids provide an asymmetric impactor population without an antihelion counterpart, making them our best candidate to resolve the sunward asymmetry. However, these impactors are both much smaller and faster than those generating the bulk of the lunar impact ejecta cloud, where  $\beta$ -meteoroids are comparable in size to the regolith particles they impact. Such an impact regime has not been previously considered for generating appreciable amounts of ejecta at the Moon. To bolster the case that  $\beta$ -meteoroids could be the culprit for the asymmetry, we consider the impact energies, total fluxes, and yield to assess the viability of this suggestion.

### 4.1. Ability to Create Ejecta

For the following calculations, we assume the grains have  $\beta = 0.6\text{--}1.2$ , corresponding to radii of  $0.5\text{--}0.2 \mu\text{m}$ , respectively, for a bulk density of  $2 \text{ g cm}^{-3}$ , and have impact speeds of  $100 \text{ km s}^{-1}$ . The bulk density assumption comes from *Helios* observations indicating a lower bulk density for a portion of  $\beta$ -meteoroid detections (Grün et al. 1980). We also assume *LDEX* detects their ejecta at a nominal altitude of 50 km, where the instrument made a large amount of its overall dust detections due to *LADEE*'s orbital geometry. While the  $\beta$ -meteoroid mass flux to the Moon is low,  $\sim 21\text{--}300 \text{ g per day}$  (compared to  $10^6 \text{ g per day}$  from meteoroids from Pokorný et al. 2019), the number fluxes to the lunar surface are significant at  $10\text{--}600 \text{ km}^{-2} \text{ s}^{-1}$ . First we compare the available energy to liberate ejecta particles. The  $\beta$ -meteoroids considered here carry  $(3\text{--}50) \times 10^{-7} \text{ J}$  of kinetic energy per impact. *LDEX* detected ejecta grains as small as  $0.3 \mu\text{m}$  in radius with an assumed silicate bulk density of  $2.5 \text{ g cm}^{-3}$  such that these grains need  $4 \times 10^{-12} \text{ J}$  of initial kinetic energy to reach their vertical turning point at 50 km, a factor of  $10^5\text{--}10^6$  less than the total available impact energy. Therefore, the  $\beta$ -meteoroid impactors carry sufficient energy to liberate the particles detectable by *LDEX*.

As the majority of the impact ejecta from submicron grains is most likely smaller than the original impactor and below *LDEX*'s detection threshold, we cannot assess the total ejecta mass yield for such a population at this time. However, we can compare the overall surface fluxes to *LDEX*'s measured impact rates. While *LDEX* did transit a small number of dense plumes registering multiple impacts per plume (Szalay & Horányi 2016a; Bernardoni et al. 2019), the majority of the measurements occurred separated by on the order of tens of

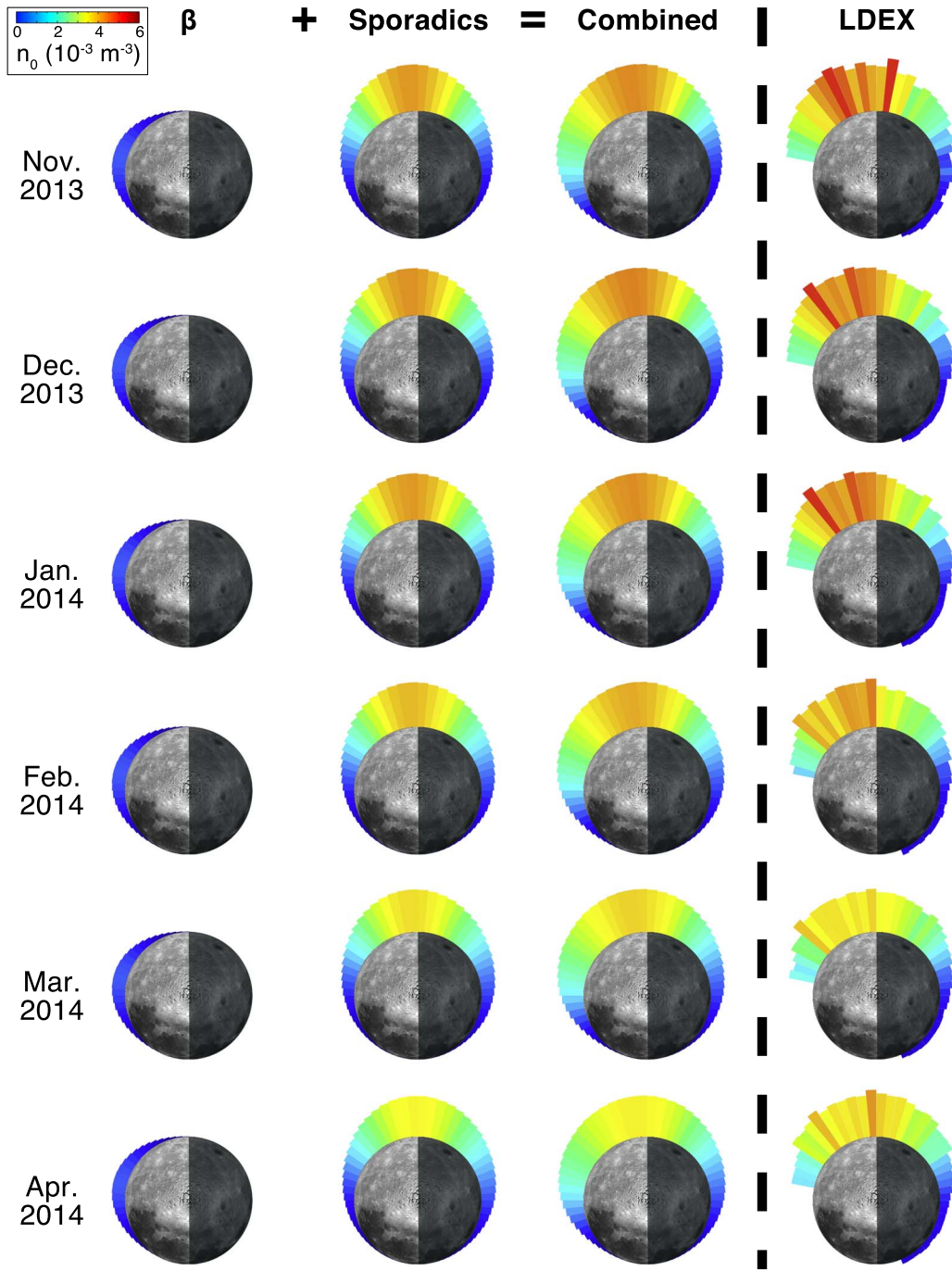


**Figure 3.** Impact ejecta production for the  $\beta$ -meteoroid and sporadic sources separately and combined, along with LDEX data from 2013 November to 2014 April. The addition of a  $\beta$ -meteoroid impactor source at a fixed location of 11 LT is able to produce the sunward-canted density distribution observed in the LDEX data.

seconds. Each of these detections is attributed to ejecta particles being generated at separate surface impact events, such that LDEX would then detect a single grain for a given lunar surface impact. Following this assumption, we compare the  $\beta$ -meteoroid fluxes to LDEX impact rates. Near the peak of the expected  $\beta$ -meteoroid ejecta production at 11 LT, LDEX measured impact rates on average of  $2 \text{ minute}^{-1}$  at 50 km altitude. If  $\beta$ -meteoroids contribute around half of these impacts as inferred in this work, that corresponds to LDEX measuring a  $\beta$ -meteoroid generated impact rate of  $1 \text{ minute}^{-1}$ . Impact plumes at the Moon were found to have small ejecta cone angles  $\sim 10^\circ$  (Bernardoni et al. 2019). At 50 km, this

corresponds to LDEX being able to detect impacts from a patch of lunar surface of  $\sim 10^3 \text{ km}^2$  below the spacecraft.  $\beta$ -meteoroids impact this amount of surface area at a rate on the order of  $10^6\text{--}10^7 \text{ minute}^{-1}$ . Therefore, to be consistent with an impact rate of  $1 \text{ minute}^{-1}$ , LDEX would only need to detect a single  $0.3 \mu\text{m}$  radius particle for every  $10^6\text{--}10^7$   $\beta$ -meteoroid impacts.

We now compare the hypothesis that small, fast impactors could generate detectable ejecta to laboratory experiments relating the impactor size and speed to the ejection speed and maximum ejected particle mass. Impact experiments into ice-silicate surfaces found  $m_{\text{max}} \leq 10^{-2} m_{\text{tot}}$ , where  $m_{\text{max}}$  is the

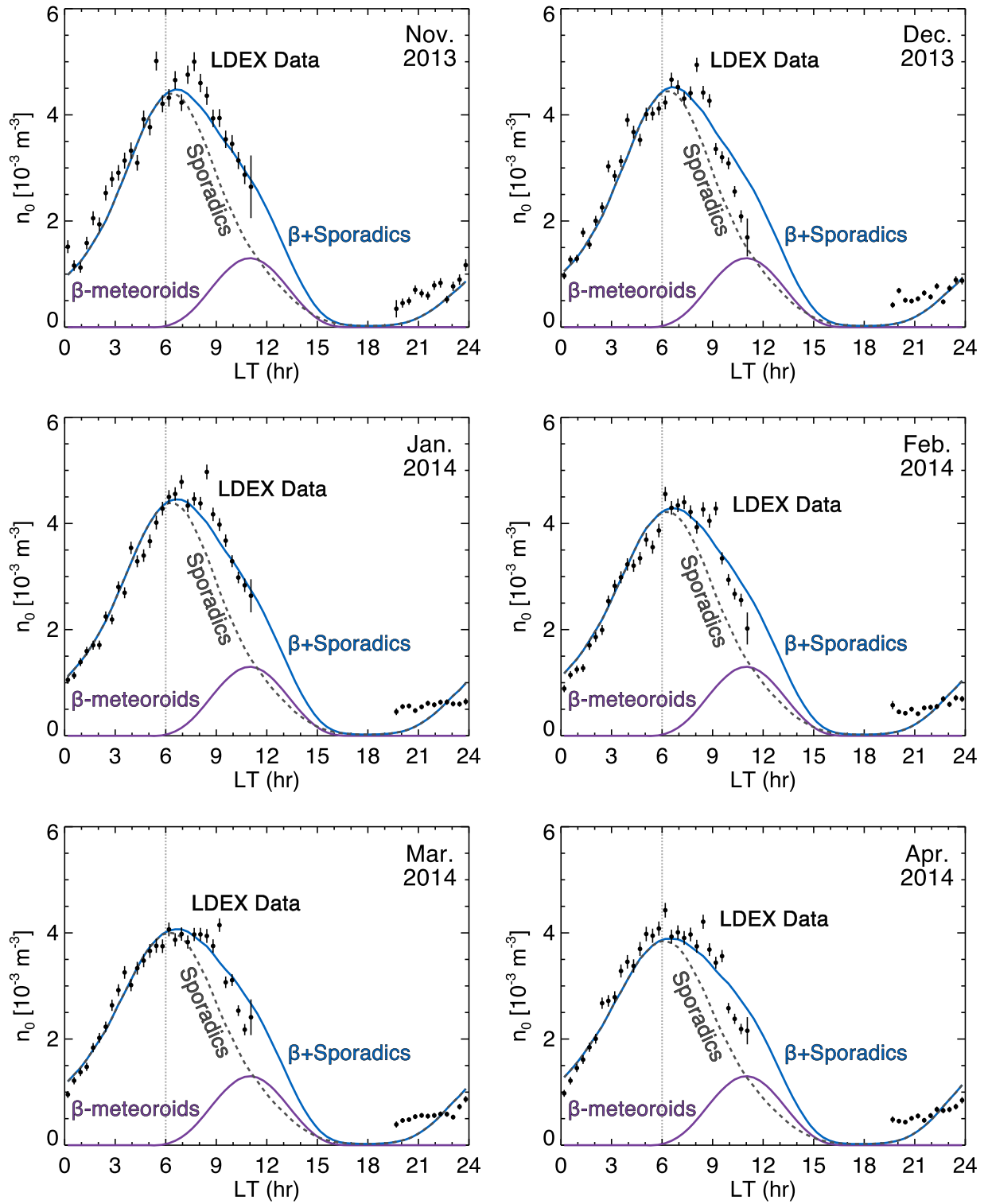


Figure 4. Impact ejecta production showing the same information displayed in Figure 3 as a function of local time (LT).

largest ejecta particle and  $m_{\text{tot}}$  is the total ejecta mass (Koschny & Grün 2001a). Assuming LDEX detects the largest mass, and that the ejecta mass is related to the impactor mass via  $m_{\text{tot}} = Ym_{\text{imp}}$  where  $Y$  is the yield, then  $m_{\text{imp}} \geq 100m_{\text{max}}/Y$ . For a range of  $m_{\text{max}}$  corresponding to  $0.3\text{--}0.7\ \mu\text{m}$  ejecta grains, lunar yields of  $Y = 20\text{--}300$  would be required to detect ejecta from  $0.5\ \mu\text{m}$   $\beta$ -meteoroids, and  $Y = 300\text{--}4,000$  from  $0.2\ \mu\text{m}$   $\beta$ -meteoroids. Lunar ejecta yields on the order of 10 from slower

and larger sporadic impactors have been inferred from LDEX data (Szalay et al. 2019b); however, much higher yields  $\gtrsim 10^3\text{--}10^4$  would be expected by extrapolating experimentally measured yields to  $100\ \text{km s}^{-1}$  impactors (Figure 10 in Koschny & Grün 2001b). The same impact experiments found that the larger ejecta particles had lower ejection speeds. To reach  $50\ \text{km}$  altitude, ejected particles need speeds of  $0.4\ \text{km s}^{-1}$ . This is less than 1% of the impactor speeds

$\sim 100 \text{ km s}^{-1}$ . Therefore, in this impactor regime, the ejecta particles detected are orders of magnitude slower than the impactors and their generation is not inconsistent with experiments. Additionally, given the lack of available experimental results for submicron, fast  $\sim 100 \text{ km s}^{-1}$  impactors, the range of possible yields is consistent with our hypothesis that these impactors could generate sufficient ejecta for LDEX to observe.

In addition to the  $\beta$ -meteoroids continually produced via collisions and/or sublimation in the inner solar system, a more intermittent source of  $\beta$ -meteoroids occurs when Sun-grazing comets or active asteroids release large quantities of dust near perihelion, most of which are released into unbound orbits (e.g., Grün & Landgraf 2001). Such sporadic occurrences would generate transient enhancements of larger  $\beta$ -meteoroids, as larger particles with lower  $\beta$  values can reach unbound orbits. Grains released at perihelion will be unbound for  $\beta \geq (1 - e_p)/2$ , where  $e_p$  is the eccentricity of the parent body (Grün et al. 1985). For example, grains with radii of  $3 \mu\text{m}$  that are 1000 times more massive than the  $\beta$ -meteoroid impactors considered in the discussion above would be able to generate significantly more ejecta mass per impact. Such grains have  $\beta = 0.06\text{--}0.3$  (Wilck & Mann 1996) and would be released on unbound orbits from parent bodies with  $e_p \geq 0.48\text{--}0.88$ , a range containing a large fraction of observed and modeled Jupiter Family Comets (Nesvorný et al. 2017). While these massive particles could generate transient ejecta enhancements, we would expect such enhancements to be highly intermittent and exhibit large variations in magnitude. However, LDEX observed its asymmetric, canted feature essentially every single orbit and did not register large density variations near the  $\beta$ -meteoroid impactor local times. Therefore, we favor the more continual flux of collision/sublimation-produced grains to be the source of ejecta production.

#### 4.2. Additional Potential Ejecta Sources

Another possible source of impactors not yet considered for lunar impacts is interstellar dust (ISD). Fluxes of ISD can reach comparable magnitudes at 1 au (e.g., Grün et al. 1993; Sterken et al. 2015; Strub et al. 2019). However, unlike  $\beta$ -meteoroids, ISD fluxes are seasonally dependent and have lower impact speeds. The peak ISD impact speed to the Moon occurs toward the end of March each year, and the *LADEE* mission ended in the middle of 2014 April. Before March, the Moon is in the “shadow” of the ISD fluxes, as solar radiation pressure can serve to repel ISDs and divert their flow around the Sun (e.g., Sterken et al. 2012). ISD impact speeds are also significantly smaller than those for  $\beta$ -meteoroids, peaking at around  $60 \text{ km s}^{-1}$  in March and decreasing to sometimes single-digit  $\text{km s}^{-1}$  magnitudes during other periods. Hence, their ability to produce impact ejecta is diminished and more variable compared to  $\beta$ -meteoroids. Their effect would be least pronounced during the late portion of the year, where LDEX still observed the sunward-canted asymmetry. Therefore, we do not expect ISDs to be responsible for this asymmetry.

Finally, we consider the family of high-speed nanodust particles that are the even smaller, nanometer-sized, brethren of  $\beta$ -meteoroids. They are likely produced by the same processes near the Sun, but their charge-to-mass ratio is sufficiently large to get them entrained in the flow of the solar wind, reaching speeds on the order of  $400 \text{ km s}^{-1}$  (Meyer-Vernet et al. 2009). The flux of nanodust near the ecliptic plane is highly variable,

as they are quickly dispersed by electromagnetic forces (Juhász & Horányi 2013), but it is estimated to be on the order of  $6 \times 10^5 \text{ km}^{-2} \text{ s}^{-1}$ , at least  $10^3$  higher than  $\beta$ -meteoroids (Czechowski & Mann 2012). However, even with their characteristically  $4\times$  higher speed, nanodust impacts deliver only a small fraction,  $\ll 0.1\%$ , of the energy of a  $\beta$ -meteoroid due their vanishingly small mass. Their small mass also indicates that nanodust impacts are unlikely to produce secondary ejecta particles detectable by LDEX, as the largest ejecta size is typically comparable to the mass of the primary impacting particle (Krivov et al. 2003). Because of their intermittent flux, which might remain absent for several weeks (Zaslavsky et al. 2012), small mass, and low impact energy, we remain in favor of  $\beta$ -meteoroids to be responsible for the sunward tilt of the lunar ejecta cloud.

#### 4.3. Potential for Future Missions

If  $\beta$ -meteoroids are in fact responsible for generating the Moon’s sunward shift in impact ejecta density, this implies that  $\beta$ -meteoroids can liberate appreciable quantities of impact ejecta at other airless bodies in the inner solar system, and by extension, at other exozodiacal bodies. At the Moon, a polar orbiting spacecraft could use the latitudinal dependence to further characterize this source (Szalay et al. 2019b). Future observations of impact ejecta at other airless bodies, for example, at (3200) Phaethon (Szalay et al. 2019a), the upcoming target of JAXA’s DESTINY+mission (Kruger et al. 2019) equipped with an in situ dust detector, could further reveal the importance of  $\beta$ -meteoroids in the evolution of airless surfaces. Additionally, these impactors could also play a role in volatile production due to meteoroid bombardment (e.g., Colaprete et al. 2016; Szalay et al. 2016). New impact ionization dust instruments have been developed that are capable of detecting fast small particles, revealing their composition, velocity vector, and mass, while looking back toward the Sun from from nearly any orbit outside the magnetosphere of the Earth, enabling a more complete exploration of  $\beta$ -meteoroids (Mocker et al. 2013; O’Brien et al. 2015).

## 5. Conclusions

Comparing impact ejecta measurements at the Moon to incident fluxes of  $\beta$ -meteoroids, we find the following conclusions:

1. The sunward-canted asymmetry of the lunar dust cloud can be explained by  $\beta$ -meteoroid impactors;
2. The detectability of the asymmetry is satisfied if LDEX can detect a single ejecta particle from only one in a million  $\beta$ -meteoroid impactors to the Moon; and
3. We propose  $\beta$ -meteoroids to be a new additional driving force for producing impact ejecta at airless bodies in the inner solar system and at other exozodiacal bodies.

J.R.S. was supported by NASA’s Lunar Data Analysis Program (LDAP), grant 80NSSC17K0702. P.P. was supported by the ISFM award. M.H. acknowledges support from NASA’s LDAP and SSERVI programs.

#### ORCID iDs

J. R. Szalay  <https://orcid.org/0000-0003-2685-9801>

P. Pokorný  <https://orcid.org/0000-0002-5667-9337>  
 M. Horányi  <https://orcid.org/0000-0002-5920-9226>

## References

- Berg, O. E., & Grün, E. 1973, in Proc of Fifteenth Plenary Meeting of COSPAR (Committee on Space Research), Space Research XIII, ed. M. I. Rycroft & S. I. Runcorn (Berlin: Akademie-Verlag), 1047
- Bernardoni, E. A., Szalay, J. R., & Horanyi, M. 2019, *GeoRL*, 46, 534
- Burns, J. A., Lamy, P. L., & Soter, S. 1979, *Icar*, 40, 1
- Colaprete, A., Sarantos, M., Wooden, D. H., et al. 2016, *Sci*, 351, 249
- Czechowski, A., & Mann, I. 2012, *Nanodust in the Solar System: Discoveries and Interpretation*, Vol. 385 (Berlin: Springer)
- Elphic, R. C., Delory, G. T., Hine, B. P., et al. 2014, *SSRv*, 185, 3
- Gault, D. E., Hoerz, F., Brownlee, D. E., & Hartung, J. B. 1974, *LPSC*, 5, 260
- Grün, E., & Landgraf, M. 2001, *SSRv*, 99, 151
- Grün, E., Pailer, N., FECHTIG, H., & Kissel, J. 1980, *P&SS*, 28, 333
- Grün, E., Zook, H. A., Baguhl, M., et al. 1993, *Natur*, 362, 428
- Grün, E., Zook, H. A., Fechtig, H., & Giese, R. H. 1985, *Icar*, 62, 244
- Horányi, M., Sternovsky, Z., Lankton, M., et al. 2014, *SSRv*, 185, 93
- Horányi, M., Szalay, J. R., Kempf, S., et al. 2015, *Natur*, 522, 324
- Janches, D., Mathews, J. D., Meisel, D. D., Getman, V. S., & Zhou, Q. H. 2000, *Icar*, 143, 347
- Janches, D., Pokorný, P., Sarantos, M., et al. 2018, *GeoRL*, 45, 1713
- Juhász, A., & Horányi, M. 2013, *GeoRL*, 40, 2500
- Koschny, D., & Grün, E. 2001a, *Icar*, 154, 402
- Koschny, D., & Grün, E. 2001b, *Icar*, 154, 391
- Krivov, A. V., Sremčević, M., Spahn, F., Dikarev, V. V., & Kholshchikov, K. V. 2003, *P&SS*, 51, 251
- Kruger, H., Strub, P., Srama, R., et al. 2019, *P&SS*, 172, 22
- Leinert, C., Richter, I., Pitz, E., & Planck, B. 1981, *A&A*, 103, 177
- Mann, I., Kimura, H., Biesecker, D. A., et al. 2004, *SSRv*, 110, 269
- Meyer-Vernet, N., Maksimovic, M., Czechowski, A., et al. 2009, *SoPh*, 256, 463
- Mocker, A., Hornung, K., Grün, E., et al. 2013, *P&SS*, 89, 47
- Nesvorný, D., Janches, D., Vokrouhlický, D., et al. 2011, *ApJ*, 743, 129
- Nesvorný, D., Vokrouhlický, D., Dones, L., et al. 2017, *ApJ*, 845, 27
- O'Brien, L., Grün, E., & Sternovsky, Z. 2015, *P&SS*, 119, 173
- Page, B., Bale, S. D., Bonnell, J. W., et al. 2020, *ApJS*, 246, 51
- Pokorný, P., Janches, D., Sarantos, M., et al. 2019, *JGRE*, 124, 752
- Pokorný, P., & Kuchner, M. 2019, *ApJL*, 873, L16
- Sterken, V. J., Altobelli, N., Kempf, S., et al. 2012, *A&A*, 538, A102
- Sterken, V. J., Strub, P., von Steiger, R., & Frisch, P. C. 2015, *ApJ*, 812, 1
- Strub, P., Sterken, V. J., Soja, R., et al. 2019, *A&A*, 621, A54
- Szalay, J. R., & Horányi, M. 2015a, *GeoRL*, 42, 580
- Szalay, J. R., & Horányi, M. 2015b, *GeoRL*, 42, 5141
- Szalay, J. R., & Horányi, M. 2016a, *Icar*, 275, 221
- Szalay, J. R., & Horányi, M. 2016b, *GeoRL*, 43, 4893
- Szalay, J. R., Horányi, M., Colaprete, A., & Sarantos, M. 2016, *GeoRL*, 43, 6096
- Szalay, J. R., Pokorný, P., Bale, S. D., et al. 2020, *ApJS*, 246, 27
- Szalay, J. R., Pokorný, P., Horanyi, M., et al. 2019a, *P&SS*, 165, 194
- Szalay, J. R., Pokorný, P., Jenniskens, P., & Horányi, M. 2018, *MNRAS*, 474, 4225
- Szalay, J. R., Pokorný, P., Sternovsky, Z., et al. 2019b, *JGRE*, 124, 143
- Wehry, A., Krüger, H., & Grün, E. 2004, *A&A*, 419, 1169
- Wehry, A., & Mann, I. 1999, *A&A*, 341, 296
- Wilck, M., & Mann, I. 1996, *P&SS*, 44, 493
- Zaslavsky, A., Meyer-Vernet, N., Mann, I., et al. 2012, *JGRA*, 117, 5102
- Zook, H. A., & Berg, O. E. 1975, *P&SS*, 23, 183